Journal of Molecular Catalysis A: Chemical 304 (2009) 71–76

Contents lists available at ScienceDirect

Journal of Molecular Catalysis A: Chemical

journal homepage: www.elsevier.com/locate/molcata

Chromium oxide catalysts for CO_x-free hydrogen generation via catalytic ammonia decomposition

L. Li [a,*], Z.H. Zhu [b,*], S.B. Wang [c], X.D. Yao [a], Z.F. Yan [d]

[a] ARC Centre for Fuctional NanoMaterials, The University of Queensland, St Lucia, QLD 4072, Australia
[b] Division of Chemical Engineering, The University of Queensland, St Lucia, QLD 4072, Australia
[c] Department of Chemical Engineering, Curtin University of Technology, GPO Box U1987, Perth, WA 6845, Australia
[d] State Key Laboratory of Heavy Oil Processing, CNPC Key Laboratory of Catalysis, China University of Petroleum, Dongying 257061, China

ARTICLE INFO

Article history:
Received 7 July 2008
Received in revised form 8 January 2009
Accepted 18 January 2009
Available online 24 January 2009

Keywords:
Hydrogen generation
Catalytic ammonia decomposition
Chromium oxide
Solid thermal decomposition

ABSTRACT

Chromium oxide nanocrystallites have been synthesized by thermal decomposition of solid precursors and evaluated as catalysts for ammonia decomposition. The physical and chemical properties of Cr_2O_3 catalysts are characterized by various techniques such as N_2 adsorption–desorption isotherms, XRD, TEM, and XPS. The relationship between catalytic activities and physicochemical and electronic properties of Cr_2O_3 catalysts is investigated. The Cr_2O_3 catalysts are active for ammonia decomposition and the activity is structure-sensitive with a close relation to particle size. During the ammonia decomposition reaction, N atoms are inserted into the Cr_2O_3 catalyst thus enhancing the activity of catalyst, due to the variation in the physical, chemical and electronic structures of Cr_2O_3 catalysts.

1. Introduction

With the extreme concerns over global warming and the depletion of fossil fuels, development of sustainable, zero-emission hydrogen technologies is the major challenge for on-board mobile applications [1]. Catalytic ammonia decomposition has been considered as one of the potential hydrogen carriers to provide CO_x-free hydrogen for fuel cells due to high energy density (3000 Wh/kg) and hydrogen capacity (17.7%), as well as CO_x-free production [2]. Currently, various metals and alloys such as Fe [3,4], Ni [5,6], Ru [7–10], Ir [11], Pt [12,13], Co [14], Rh [6,11,15] and $Zr_{1-x}Ti_xM_1M_2$ (M_1, M_2 = Cr, Mn, Fe, Co, Ni; x = 0–1) [16], and compounds of nitrides and carbides including MoN_x, VN_x, VC_x and MoC_x [17–20] have been tested for ammonia decomposition and Ru metal is regarded as the most active metal catalyst. Previous studies on ammonia decomposition over various supported metal catalysts suggested Ru catalysts supported on different carbon materials (such as activated carbon, carbon nanotubes (CNTs) and CNTs-MgO) showed the highest catalytic activity for ammonia decomposition among supported metal catalysts [21–23]. However, cracking ammonia to hydrogen over the Ru-based catalysts usually begins at temperatures of 450–550 °C, which makes the carbon supports form methane under H_2 atmosphere. The rate and extent of ammonia decomposition in this process are not satisfactory for practical fuel cell application. In addition, high cost of Ru metal limits its practical usage in fuel cells. Recently, researchers have made great efforts to seek inexpensive alternatives, especially Ni, to Ru catalysts. Ganley et al. [6] investigated the activity of ammonia decomposition on Ni/Al_2O_3 catalysts and found that NH_3 conversion of the Ni catalyst is only 39%. A similar result was reported by Li et al. [24]; 7% Ni/SiO_2 catalyst only exhibited 13% ammonia conversion at 550 °C. It is thus indicated that the activity of ammonia decomposition on Ni catalysts is much lower than that of Ru catalysts. It cannot be satisfactory for fuel cell application even at high temperature. Moreover, metal catalysts for ammonia decomposition may produce significant amounts of hydrazine [25]. Therefore, it is important to find alternative active catalysts for ammonia decomposition.

Chromium oxide and supported chromium oxide catalysts have good performance in dehydrogenation and selective catalytic reduction of NO_x with ammonia. However, ammonia decomposition on Cr_2O_3 or supported Cr_2O_3 catalysts has never been reported so far. In this paper, synthesis of chromium oxide (Cr_2O_3) nanocrystallites and their performance in ammonia decomposition are reported. The correlation between the physicochemical and structural properties and catalytic activity of chromium oxide catalyst was comprehensively analyzed. The electronic properties of fresh and used Cr_2O_3 catalysts were characterized by X-ray photoelectron spectroscopy (XPS) technique and the reaction mechanism and kinetics of ammonia decomposition over the Cr_2O_3 catalyst were also discussed.

* Corresponding authors.
E-mail addresses: l.li2@uq.edu.au (L. Li), z.zhu@uq.edu.au (Z.H. Zhu).

1381-1169/$ – see front matter © 2009 Elsevier B.V. All rights reserved.
doi:10.1016/j.molcata.2009.01.026

2. Experimental

2.1. Synthesis of chromium oxide

Chromium oxide catalysts were synthesized according to the procedures as described by Li et al. [26]. In a typical synthesis, $Cr(NO_3)_3{\cdot}9H_2O$ powders were fully mixed with cetyltrimethylammonium bromide (CTAB) surfactant. The mixture was transferred into autoclaves and then put into the oven at 140–200 °C for 24 h. After heating, the obtained samples were washed with distilled water and dried at room temperature. The chromium oxide samples obtained at different decomposition temperatures were designated as Cr-CTAB-T (T represents the decomposition temperature).

2.2. Catalytic testing

The reaction of ammonia decomposition was carried out in a fixed-bed flow reactor [27]. A 0.2-g (60–80 mesh) catalyst was placed in the central section of a reactor. Prior to the reaction, the as-synthesized Cr_2O_3 samples were calcined at 600 °C under air flow for 5 h and then were purged with Ar flow (purity > 99.99%) for 1 h. The calcined samples were cooled down to the desired reaction temperature in the range of 400–600 °C under Ar flow and then the flow was changed to pure ammonia gas. The gas hourly space velocity ($GHSV_{NH3}$) is 60000 ml/(h g_{cat}). The calcined chromium oxide catalysts were designated as Cr-CTAB-T-600.

The GC technique provided quantitative data for H_2 and N_2 components. The NH_3 conversion was calculated from the mole fraction of H_2 (y_{H_2}) in the products according to the following equation:

$$X_{NH_3} = \frac{2y_{H_2}}{3 - 2y_{H_2}} \quad (1)$$

These integral conversion results were then fit with polynomials to generate equations that could be analytically differentiated to obtain ammonia decomposition rates as a function of conversion (and hence species partial pressures). According to Ref. [28], the ammonia decomposition reaction is a first-ordered reaction and the equation describing a rate of the ammonia decomposition is in the following form:

$$r = kc_{NH_3} \quad (2)$$

where k is the reaction rate constant, depending on the temperature, and c_{NH_3} is the concentration of ammonia. The apparent activation energy (E_a) can be determined by fitting the equation to the conversion data as a function of reaction temperature with the following equation:

$$r = A\exp\left(-\frac{E_a}{RT}\right)c_{NH_3} = \frac{c^o_{NH_3}X_{NH_3}}{t} \quad (3)$$

2.3. Catalytic characterization

Powder X-ray diffraction (XRD) measurements were conducted on a Bruker D8 advanced research XRD with Cu Kα radiation at a scanning rate of 2°/min in the 2θ range from 10° to 80°. The Cr_2O_3 samples after calcination were measured on a mini Rigaku XRD with Co Kα radiation at a scanning rate of 2°/min in the 2θ range from 10° to 80°. The average crystallite size, D_c, was calculated using the Scherrer equation $D_c = 0.9\lambda/(\beta\cos\theta)$, where λ is the wavelength of the Cu or Co Kα radiation, β is the peak full width at half-maximum intensity of the most intense peak in the pattern, corrected for instrumental broadening.

The BET surface areas and textural structure were measured by nitrogen adsorption–desorption isotherms using an automated adsorption analyzer (Autosorb-1C, Quantachrome, USA). Prior to N_2 adsorption measurement, the samples were degassed at 200 °C for 6 h. Surface areas of the samples (S_{BET}) were obtained from the BET equation, which was applied in relative pressure range from 0.05 to 0.25. The total pore volume was derived from the adsorption amount at a relative pressure of 0.98. The average particle size, D_p, was estimated using the equation $D_p = 6/\rho S_{BET}$, where S_{BET} is the BET surface area of Cr_2O_3 samples and ρ is the density of the primary bulk phase ($\rho = 5.21$ g/cm^3) [17–19].

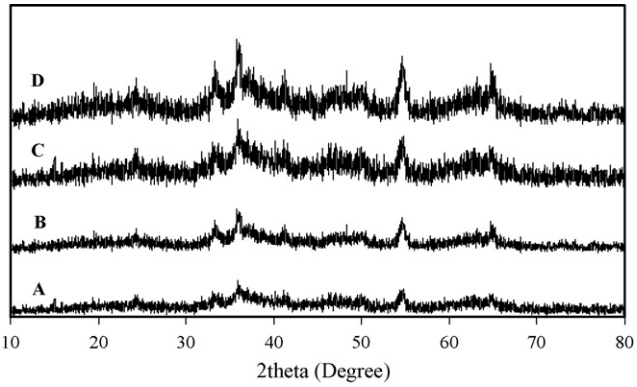

Fig. 1. The XRD patterns of as-synthesized Cr_2O_3 samples at different decomposition temperatures (A. Cr-CTAB-140; B. Cr-CTAB-160; C. Cr-CTAB-180; D. Cr-CTAB-200).

The XPS measurements were conducted using a PHI-560 ESCA system (Perkin-Elmer). All spectra were acquired at a basic pressure 2×10^{-7} Torr with Mg Kα excitation at 15 kV and recorded in the ΔE = constant mode, at pass energies of 50 and 100 eV.

The morphology and particle size of Cr_2O_3 catalysts were determined by transmission electron microscopy in JEOL-1010 electron microscope at 200 keV. Before the TEM measurements, the specimens were ground in ethanol and supported on holey carbon films located on Cu grids.

3. Results

3.1. The characterization of Cr_2O_3 nanocrystallites

The XRD patterns of Cr_2O_3 samples obtained at different decomposition temperatures are shown in Fig. 1. All of the as-synthesized Cr_2O_3 samples have rhombohedral structure and are presented as α-phase, which belongs to the $R\bar{3}c$ space group with lattice parameters $a = 4.958$ Å and $c = 13.594$ Å, as reported in our previous work [29]. The crystallite sizes (D_c) of these samples are around 10–15 nm, suggesting that the inorganic framework consists of Cr_2O_3 nanocrystallites. This rhombohedral unit cell contains six Cr_2O_3 molecules close-packed in a hexagonal pattern with alternate layers of chromium and oxygen atoms in planes perpendicular to the z direction, generating oxygen defect structure. Both chromium and oxygen species tend to acquire the highest possible coordination numbers during the reaction process. Accordingly, the α-Cr_2O_3 rhombohedral structure is very important in catalysis.

Nitrogen adsorption–desorption isotherms of synthesized Cr_2O_3 samples in Fig. 2 exhibited type-IV isotherms with H3 hysteresis loops, indicating that the Cr_2O_3 samples possess slit mesopores. More quantitative results are presented in Table 1. The

Table 1
Textural properties of Cr_2O_3 samples at different temperatures.

Sample	S_{BET} (m^2/g)	V_{tot} (cm^3/g)	Pore size (nm)	D_p (nm)
Cr-CTAB-140	138	0.131	3.8	8.3
Cr-CTAB-160	125	0.267	8.6	9.2
Cr-CTAB-180	142	0.265	7.5	8.1
Cr-CTAB-200	143	0.268	7.5	8.1

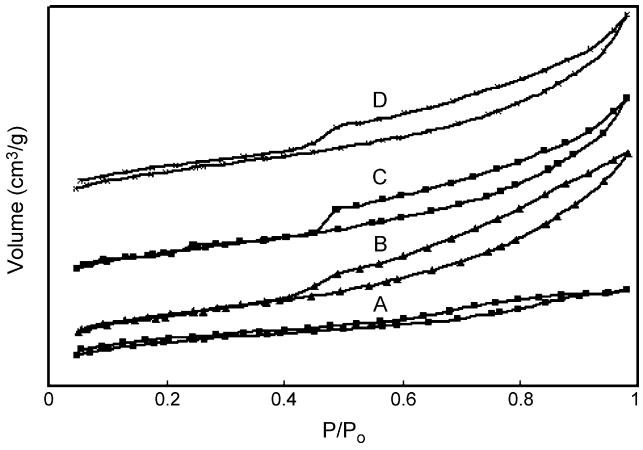

Fig. 2. The nitrogen adsorption–desorption isotherms of Cr_2O_3 samples (A. Cr-CTAB-140; B. Cr-CTAB-160; C. Cr-CTAB-180; D. Cr-CTAB-200).

Table 2
Physical properties of Cr_2O_3 samples after calcination.

Sample	S_{BET} (m^2/g)	V_{tot} (cm^3/g)	Pore size (nm)	D_p (nm)	D_c (nm)
Cr-CTAB-140-600	44	0.384	34.9	26.2	28.8
Cr-CTAB-160-600	43	0.368	33.9	26.5	21.8
Cr-CTAB-180-600	39	0.230	27.6	29.3	31.0
Cr-CTAB-200-600	34	0.260	30.6	34.1	34.3

synthesized Cr_2O_3 samples have large BET surface areas in the range of 125–143 m^2/g and pore volume in the range of 0.131–0.268 m^3/g, which are much larger than those of bulk Cr_2O_3 (20–27 m^2/g) [30,31]. These short channels, large pore volume and nanocrystallite size may be conducive to high activity and conductivity in catalytic and electromagnetic materials, respectively, because of less resistance to mass transport and charge-transfer process.

Fig. 3 shows the XRD patterns of Cr_2O_3 catalysts calcined at 600 °C for 5 h (Co Kα radiation). As seen from the XRD patterns, the particle sizes of Cr_2O_3 catalysts increased after calcination, suggesting the particle aggregation of nanosized Cr_2O_3 catalysts and structural shrink during calcining process. The crystallite sizes (D_c) of Cr_2O_3 catalysts after calcination are around 20–35 nm as listed in Table 2. A comparison of the crystallite size with the particle size of Cr_2O_3 catalyst shows that the Cr_2O_3 particle is composed of the Cr_2O_3 crystal, as demonstrated by the TEM image of Cr_2O_3-CTAB-200-600 catalyst shown in Fig. 4.

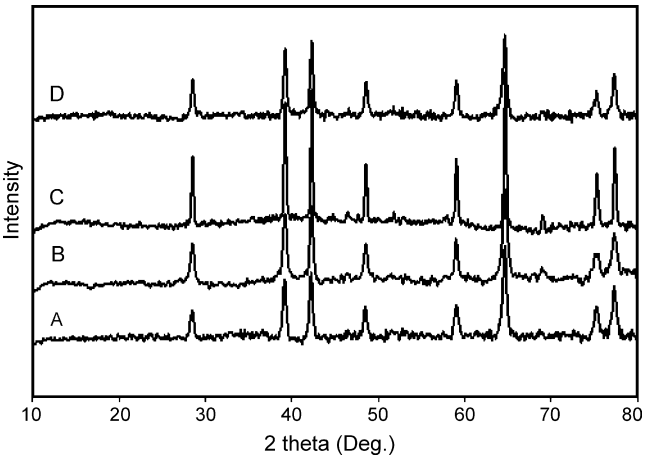

Fig. 3. The XRD patterns of Cr_2O_3 catalysts after calcination (A. Cr-CTAB-140-600; B. Cr-CTAB-160-600; C. Cr-CTAB-180-600; D. Cr-CTAB-200-600).

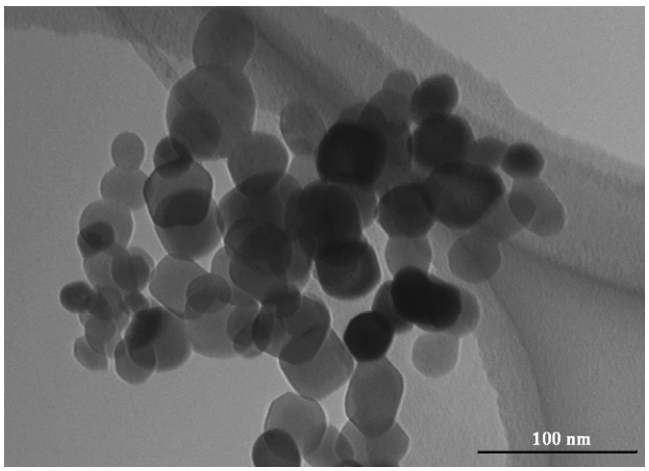

Fig. 4. TEM image of Cr-CTAB-200-600 catalyst.

The textural and physical properties of the Cr_2O_3 catalysts are also listed in Table 2. One can see that calcination treatment at 600 °C results in a significant decrease in surface area, due to the collapse of small pore and the growth of Cr_2O_3 nanocrystallites. However, the Cr_2O_3 catalysts after calcination have larger pore volume and pore size than the as-synthesized Cr_2O_3 samples. This is probably because of sintering and aggregation of the Cr_2O_3 particles to form larger voids in the Cr_2O_3 samples. These larger pore volume and larger pores are beneficial to mass transport for catalytic reaction.

3.2. Catalytic activities of NH_3 decomposition on Cr_2O_3 catalysts

Fig. 5 shows the catalytic activities of Cr_2O_3 catalysts on NH_3 decomposition at 600 °C ($GHSV_{NH_3}$ = 60, 000 ml/(h g_{cat})). The ammonia conversion on fresh Cr_2O_3 catalysts increases at the initial stage and then becomes stable after 2 h reaction, which is ascribed to a slow nitridization of the Cr_2O_3 catalysts, confirmed by XPS results shown later (see Figs. 11 and 12). Table 3 lists the activities of the Cr_2O_3 catalysts after calcination at 600 °C. The ammonia conversion over the Cr_2O_3 catalysts is 37.9–43.4% and the rate of hydrogen generation is 11.6–13.3 mmol/min g_{cat} at 600 °C, suggesting that Cr_2O_3 catalysts are active for ammonia decomposition.

The catalytic performance of Cr_2O_3 catalysts for ammonia decomposition as a function of the reaction temperature is shown in Fig. 6. The NH_3 conversion on Cr-CTAB-200-600 catalyst remarkably increased as reaction temperature rose from 450 to 600 °C, in

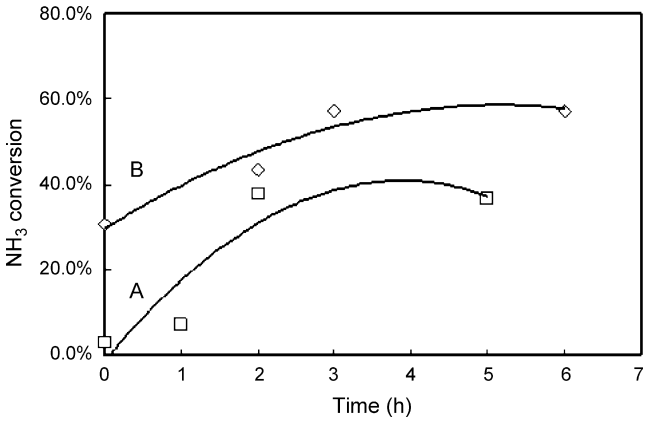

Fig. 5. NH_3 conversions versus time over different Cr_2O_3 catalysts at 600 °C (A. Cr-CTAB-180-600; B. Cr-CTAB-200-600) [$GHSV_{NH_3}$ = 60, 000 ml/(h g_{cat})].

Table 3
NH_3 conversion and H_2 formation rate over Cr_2O_3 catalysts at 600 °C.

Catalysts	NH_3 conversion (%)	H_2 formation rate (mmol/min g_{cat})	Reference
Cr-CTAB-140-600	37.9%	11.6	This work
Cr-CTAB-160-600	43.4%	13.3	This work
Cr-CTAB-180-600	38.7%	11.9	This work
Cr-CTAB-200-600	42.6%	13.1	This work
10%Ni/SiO_2-600	36.4%	11.4	[2]
5%Ru/SiO_2-550	96.5%	32.3	[36]

accordance with endothermic process ($\Delta H = 46$ kJ/mol) of ammonia decomposition reaction. As is known, ammonia decomposition is the first-order reaction. As shown in Fig. 7, the apparent activation energy of 70.6 ± 5 kJ/mol was estimated at 450–600 °C, in good agreement with activation energies for metal catalysts [32]. Similar activation energies indicate a similar rate-determining step of the reaction on Cr_2O_3 catalysts and metal-based catalysts.

In addition, the stability of the Cr-CTAB-200–600 catalyst was investigated at a space velocity of $GHSV_{NH_3} = 60,000\ ml/(h\,g_{cat})$ within a 125-h period. The catalytic activity of ammonia decomposition and H_2 rate formation (Fig. 8) remained relatively constant at 600 °C until 90 h. The conversion shows a slower decrease rate after 90 h, demonstrating that Cr_2O_3 catalyst is thermally stable.

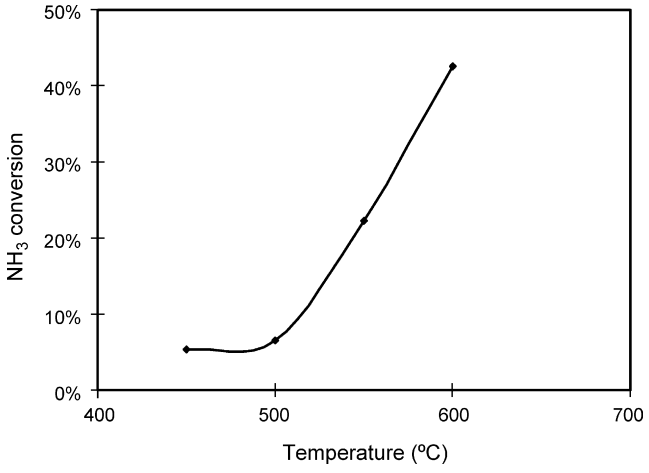

Fig. 6. NH_3 conversions on the Cr-CTAB-200-600 catalyst at different reaction temperatures.

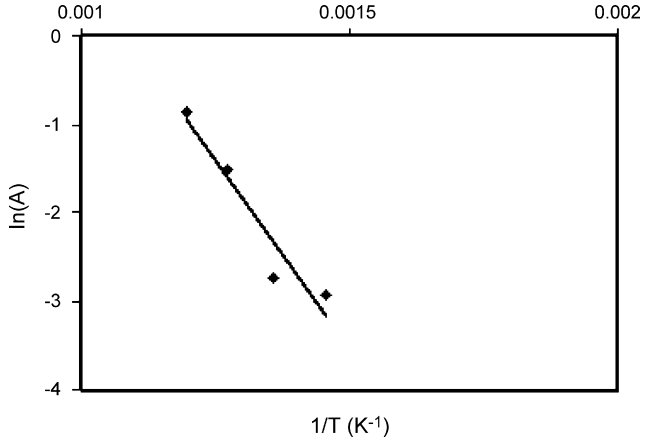

Fig. 7. The Arrhenius plots over Cr-CTAB-200-600 catalyst [$GHSV_{NH_3} = 60,000\ ml/(h\,g_{cat})$].

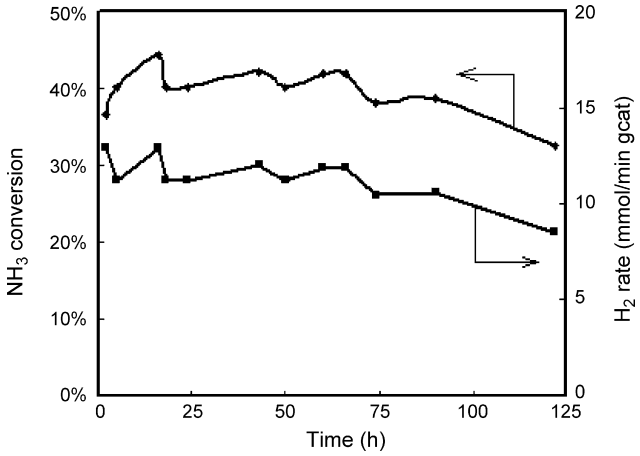

Fig. 8. Catalyst stability of Cr-CTAB-200-600 catalyst at 600 °C [$GHSV_{NH_3} = 60,000\ ml/(h\,g_{cat})$].

4. Discussion

4.1. Structure-sensitivity

As shown in Fig. 9, the activities of Cr_2O_3 catalysts for ammonia decomposition increase with increasing grain size of Cr_2O_3 nanocrystallite except Cr-CTAB-160-600 catalyst, indicating that the ammonia conversion on Cr_2O_3 catalysts is closely related to the particle size of Cr_2O_3 catalyst.

To further understand the particle-size effect on catalytic activities of Cr_2O_3 catalysts, the relationship between catalytic activities and population of crystallographic surface sites (associated with atoms at edges, kinks, and vertices) was investigated and shown in Fig. 10. The catalytic activity normalized by the surface area is inversely related to the grain boundary that is proportional to $D_p/(D_c)^2$ (particle size D_p was obtained from the BET surface area estimated by N_2 adsorption, and crystallite size D_c was obtained from the Scherrer equation in XRD). Alternatively, the activity normalized by the surface area increases as the grain boundary length decreases. Therefore, the active sites of Cr_2O_3 catalysts are more likely to reside on the more ordered Cr_2O_3 particle surface instead of defective particle surface.

We note that Cr-CTAB-160-600, which is not included in Figs. 9 and 10, has the highest activity. It is also noted that the crystallite size D_c of this sample is the lowest. The correlation between

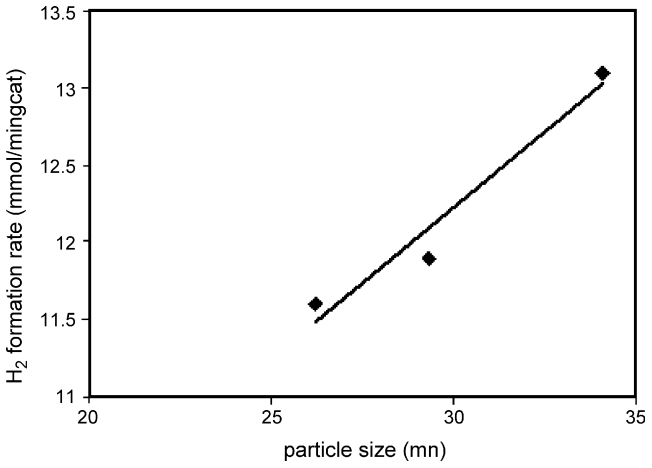

Fig. 9. The catalytic activities of Cr-CTAB-T-600 catalysts with particle size ($T = 140$, 180 and 200 °C).

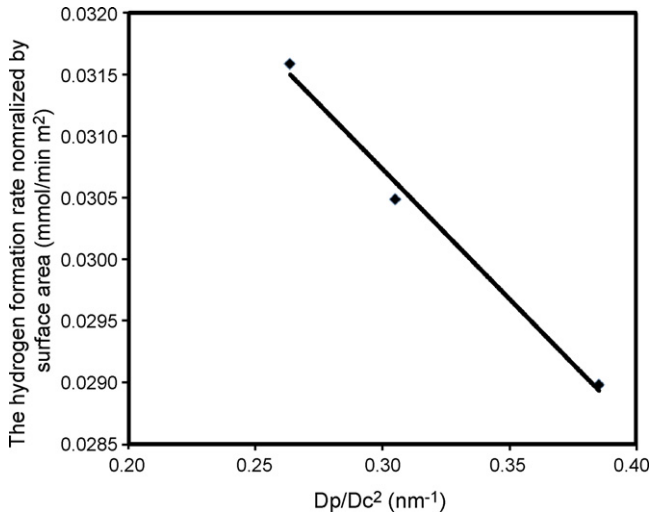

Fig. 10. The catalytic properties of the Cr-CTAB-T-600 catalysts with a derivation between particle size and crystallite size (T = 140, 180 and 200 °C).

the high activity and the low D_c value is not clear yet, and on-going research is being carried out to clarify it.

4.2. Preliminary mechanism studies of ammonia decomposition on Cr_2O_3 catalysts

In order to find out the relationship between catalytic activity and electronic structure of Cr_2O_3 catalysts and the mechanism of ammonia decomposition thereon, we investigated the surface properties of Cr_2O_3 catalysts by the XPS technique. Fig. 11 presents the survey of fresh and used Cr_2O_3 catalysts. The N 1s peak appeared in the used Cr_2O_3 catalyst surface and the intensities of oxygen species on the used Cr_2O_3 catalysts were lower than those on fresh Cr_2O_3 catalysts, indicating that nitrogen atoms replace part of oxygen atoms on the Cr_2O_3 lattice during the ammonia decomposition reaction. This is also confirmed by the XPS spectra of N 1s and Cr 3d (shown in Fig. 12). As shown in Fig. 12a and b, the Cr 3d peak of the fresh Cr_2O_3 catalyst (576.1 eV) was split into two peaks for the used Cr_2O_3 catalyst. These two Cr 3d peaks are ascribed to the Cr_2O_3 phase (576.0 eV) and the Cr_2N phase (574.8 eV). Moreover, the N 1s XPS spectra shown in Fig. 12c confirmed the existence of the Cr_2N phase (397.4 eV) on the surface of the Cr_2O_3 catalysts used for ammonia decomposition. The other N 1s peak at 399.5 eV is

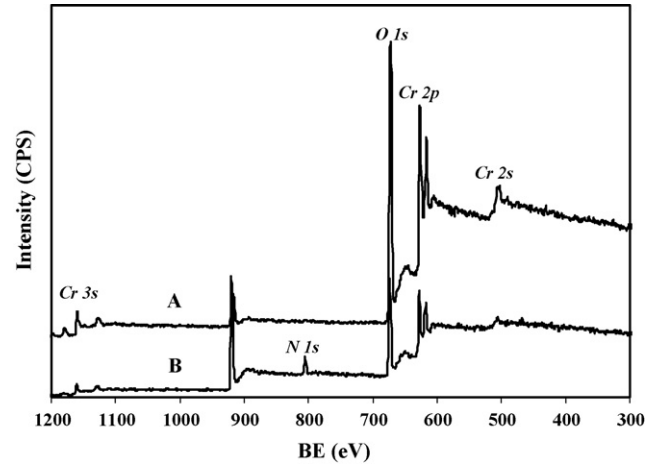

Fig. 11. The typical surveys of XPS spectra for fresh and used Cr-CTAB-200-600 catalysts (A. fresh Cr_2O_3 catalyst; B. used Cr_2O_3 catalyst).

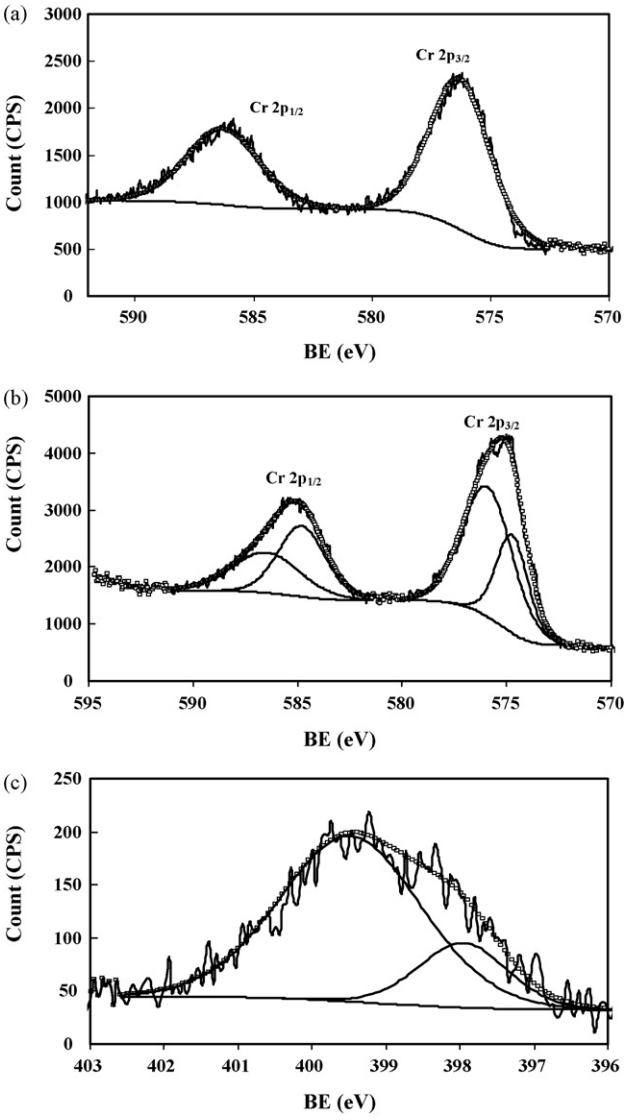

Fig. 12. The XPS spectra of Cr 3d and N 1s for Cr-CTAB-200-600 catalyst. (a) Cr 3d XPS spectra of fresh, (b) used Cr-CTAB-200-600 catalyst and (c) N 1s XPS spectra of used Cr-CTAB-200-600 catalyst.

ascribed to a nitrogen ligand with metal. These results suggest that nitrogen atoms are inserted into the crystal lattice of Cr_2O_3 catalysts to form the chromium nitride compounds, verifying the above speculation of a slow nitridation during the ammonia decomposition process. The slow nitridation was also observed for V, W, and Mo metals in catalytic reactions during nitriding [33–35].

By comparing the XPS results and catalytic activities at different reaction temperatures, it can be found that interstitial CrN_xO_y compounds formed in Cr_2O_3 catalysts above 550 °C enhanced the catalytic activities of ammonia decomposition, suggesting CrN_xO_y compounds are the active sites for ammonia decomposition. Interstitial CrN_xO_y formation increased the metal oxide bond distance, resulting in expansion of the Cr_2O_3 lattice and variation in the electronic, physical and chemical properties of the host metal oxide. In Cr_2O_3 bulks, nitrogen introduction caused the formation of oxygen-deficient catalysts, resulting in geometrical irregularities such as kinks, dislocations and vacancies in these catalysts. The existence of deficiencies may cause improvement of catalytic activities. On the other hand, since nitrogen is less electronegative than oxygen, interstitial CrN_xO_y compounds should be less acidic than the original Cr_2O_3 catalysts, which would help the recombination of N atoms

to N_2. Nitrogen introduction weakens the Cr–O bond and should be beneficial for recombinative desorption of surface nitrogen atoms on the Cr_2O_3 surface, making their catalytic activities similar to those of Pt and Ru.

Previous studies proposed that N–H bond cleavage and recombinative desorption of surface nitrogen atoms are slow steps in NH_3 decomposition. In combination with the previous discussion and XPS results, we conclude that when ammonia decomposition takes place on the surface of Cr_2O_3 catalysts, ammonia is activated to break the N–H on the Cr_2O_3 surfaces. Subsequently, nitrogen atoms on the active site are formed by consecutive reactions from dissociation of NH_x. Finally, surface nitrogen atoms are recombined together to form N_2 and part of nitrogen atoms enter into the Cr_2O_3 lattice.

4.3. Comparison between catalytic properties of Cr_2O_3 catalysts and other systems

Table 3 shows that Cr_2O_3 catalysts prepared in this study are more active than 10% Ni/SiO_2 catalyst but much less active than the Ru-based catalyst previously reported [2,36]. Cr_2O_3 catalysts have higher E_a than the Ru/CNTs catalysts with the E_a value of 69.4 kJ/mol, thus resulting in lower catalytic activity. In addition, recombination of nitrogen is inhibited on Cr_2O_3 surface because of the strong Cr–N bond formation when ammonia is adsorbed on the Cr_2O_3 surface. Therefore, addition of other components to weaken the interaction of Cr–N in Cr_2O_3 systems should improve the catalytic activity of ammonia decomposition. Currently, many investigations have found that addition of a promoter to the catalyst systems significantly increases the activity. For Ru/C, Cs and Ba have been reported to produce stronger promotion effect in ammonia decomposition [37,38]. Au and coworkers [16] systematically investigated the effects of promoting cations such as rare earth, alkali, and alkaline earth metal on the catalytic activity of Ru/CNTs and found that alkali or alkali earth metal ions are efficient promoters for supported Ru catalysts in the synthesis and decomposition of NH_3 and that K would be the best promoter. Thus, it would be possible to further enhance the catalytic activities of Cr_2O_3 catalysts by modifying with various promoters and the research is being carried out in our group.

5. Conclusion

Mesoporous Cr_2O_3 catalysts were successfully synthesized by solid thermal decomposition using CTAB surfactant and evaluated for NH_3 decomposition. It is found that the activities of NH_3 decomposition on Cr_2O_3 catalysts increases as the particle size of Cr_2O_3 catalysts increases, suggesting that NH_3 decomposition on Cr_2O_3 catalysts is structure-sensitive and the most active catalyst has a large particle size. XPS results indicate that nitrogen atoms were introduced to the Cr_2O_3 lattice and formed interstitial CrN_xO_y compounds, resulting in the changes in physical, chemical and electronic structures of Cr_2O_3 catalysts. Interstitial CrN_xO_y compounds are formed during the reaction and play as the active sites for ammonia decomposition. Moreover, the catalysts exhibit stable activity.

References

[1] L. Schlapbach, A. Zuttel, Nature 414 (2001) 353–358.
[2] T.V. Choudhary, C. Sivadinarayana, D.W. Goodman, Catal. Lett. 72 (2001) 197–201.
[3] Y. Ohtsuka, C.B. Xu, D.P. Kong, N. Tsubouchi, Fuel 83 (2004) 685–692.
[4] A. Jedynak, Z. Kowalczyk, D. Szmigiel, W. Raróg, J. Zieliński, Appl. Catal. A 237 (2002) 223–226.
[5] T.V. Choudhary, C. Sivadinarayana, D.W. Goodman, Chem. Eng. 93 (2003) 69–80.
[6] J.C. Ganley, F.S. Thomas, E.G. Seebauer, R.I. Masel, Catal. Lett. 96 (2004) 117–122.
[7] K. Hashimoto, N. Toukai, J. Mol. Catal. A 161 (2000) 171–178.
[8] S.P. Sheu, H.G. Karge, R. Schlogl, J. Catal. 168 (1997) 278–291.
[9] W. Tsai, W.H. Weinberg, J. Phys. Chem. 91 (1987) 5302–5307.
[10] S.F. Yin, B.Q. Xu, C.F. Ng, C.T. Au, Appl. Catal. B 48 (2004) 237–241.
[11] G. Papapolymerou, V. Bontozoglou, J. Mol. Catal. A 120 (1997) 165–171.
[12] A.J. Robertso, E.M. Willhoft, Trans. Faraday Soc. 63 (1967) 476.
[13] J.J. Vajo, W. Tsai, W.H. Weinberg, J. Phys. Chem. 89 (1985) 3243–3251.
[14] W. Raróg-Pilecka, A. Jedynak-Koczuk, J. Petryk, E. Miśkiewicz, S. Jodzis, Z. Kaszkur, Z. Kowalczyk, Appl. Catal. A 300 (2006) 181–185.
[15] A. Vavere, R.S. Hansen, J. Catal. 69 (1981) 158–171.
[16] S.F. Yin, B.Q. Xu, X.P. Zhou, C.T. Au, Appl. Catal. A 277 (2004) 1–9.
[17] J.G. Choi, Appl. Catal. A 184 (1999) 189–201.
[18] J.G. Choi, J. Catal. 182 (1999) 104–116.
[19] J.G. Choi, J. Ha, J.W. Hong, Appl. Catal. A 168 (1998) 47–56.
[20] C.H. Liang, W.Z. Li, Z.B. Wei, Q. Xin, C. Li, Ind. Eng. Chem. Res. 39 (2000) 3694–3697.
[21] W. Raróg, Z. Kowalczyk, J. Sentek, D. Składanowski, D. Szmigiel, J. Zieliński, Appl. Catal. A 208 (2001) 213–216.
[22] W. Raróg-Pilecka, D. Szmigiel, A. Komornicki, J. Zieliński, Z. Kowalczyk, Carbon 41 (2003) 589–591.
[23] R.Z. Sorensen, L.J.E. Nielsen, S. Jensen, O. Hansen, T. Johannessen, U. Quadde, C.H. Christensen, Catal. Commun. 6 (2005) 229–232.
[24] X.K. Li, W.J. Ji, J. Zhao, S.J. Wang, C.T. Au, J. Catal. 236 (2005) 181–189.
[25] H. Soerijanto, C. Rödel, U. Wild, M. Lerch, R. Schomäcker, R. Schlögl, T. Ressler, J. Catal. 50 (2007) 19–24.
[26] L. Li, Z.H. Zhu, X.D. Yao, G.Q. Lu, Z.F. Yan, Micro. Meso. Mater. 112 (2008) 621–626.
[27] L. Li, Z.H. Zhu, G.Q. Lu, Z.F. Yan, S.Z. Qiao, Carbon 45 (2007) 11–20.
[28] L. Li, Z.F. Yan, G.Q. Lu, Z.H. Zhu, J. Phys. Chem. B 110 (2006) 178–183.
[29] W. Arabczyk, J. Zamynny, Catal. Lett. 24 (1994) 197.
[30] S.D. Rossi, G. Ferraris, S. Fremiotti, E. Garrone, G. Ghiotti, M.C. Campa, V. Indovina, J. Catal. 148 (1994) 36–46.
[31] M. Cherian, M.S. Rao, W.T. Yang, J.M. Jehng, A.M. Hirt, G. Deo, Appl. Catal. A 233 (2002) 21–33.
[32] W.Q. Zheng, J. Zhang, H.Y. Xu, W.Z. Li, Catal. Lett. 119 (2007) 311–318.
[33] R.B. Levy, M. Boudart, Science 81 (1973) 547–549.
[34] J.H. Sinfelt, D.J.C. Yates, Nature (London), Phys. Sci. 229 (1971) 27.
[35] S.R. Logan, C. Kemball, Trans. Faraday Soc. 56 (1960) 144–153.
[36] S.Y. Yin, B.Q. Xu, W.X. Zhu, C.F. Ng, X.P. Zhou, C.T. Au, Catal. Today 93 (2004) 27–38.
[37] W. Raróg-Pilecka, D. Szmigiel, Z. Kowalczyk, S. Jodzis, J. Zielinski, J. Catal. 218 (2003) 465–469.
[38] R.Z. Sorensen, A. Klerke, U. Quaade, S. Jensen, O. Hansen, C.H. Christensen, Catal. Lett. 112 (2006) 77–81.